Journal of Power Sources 185 (2008) 727–733

Contents lists available at ScienceDirect

Journal of Power Sources

journal homepage: www.elsevier.com/locate/jpowsour

Electrocatalysts for bifunctional oxygen/air electrodes

V. Nikolova[a], P. Iliev[a], K. Petrov[a], T. Vitanov[a,*], E. Zhecheva[b], R. Stoyanova[b], I. Valov[c], D. Stoychev[c]

[a] Institute of Electrochemistry and Energy Systems, Bulgarian Academy of Sciences, Acad. G.Bonchev Street, bl.10., Sofia 1113, Bulgaria
[b] Institute of General and Inorganic Chemistry, Bulgarian Academy of Sciences, G. Bonchev Street, bl.11., Sofia 1113, Bulgaria
[c] Institute of Physical Chemistry, Bulgarian Academy of Sciences, Acad. G.Bonchev Street, bl. 11, Sofia 1113, Bulgaria

ARTICLE INFO

Article history:
Received 21 March 2008
Received in revised form 16 July 2008
Accepted 3 August 2008
Available online 22 August 2008

Keywords:
Bifunctional air/oxygen electrode
Gas diffusion electrodes
Oxygen reduction and evolution
Electrocatalysts
Cobalt oxides

ABSTRACT

Oxygen reduction and evolution have been studied with respect to the development of bifunctional air/oxygen electrode (BFE). Three groups of catalysts have been prepared: (i) $Cu_xCo_{3-x}O_4$ by thermal decomposition of mixed nitrate and carbonate precursors; (ii) thin films of Co–Ni–Te–O and Co–Te–O were deposited by vacuum co-evaporation of Co, Ni and TeO_2 and (iii) Co_xO_v/ZrO_2 films were obtained by electrochemical deposition.

The electrochemical behavior of the chemically synthesized catalysts was studied on classical bilayered gas diffusion electrodes (GDEs), where the catalyst is in form of powder. The GDE catalyzed with vacuum deposited catalysts was prepared by direct deposition of the catalyst on gas-supplying layer, thus creating a ready-to-use gas diffusion electrode. Catalysts prepared electrochemically were first deposited on Ni foam and than pressed onto the gas-supplying layer.

Different catalysts deposited on classical and originally designed GDEs were compared by their electrochemical performances. $Cu_{0.3}Co_{2.7}O_4$ deposited on a classical bilayered GDE with loading of 50 mg cm^{-2} exhibits stable current–voltage characteristics after 200 charge–discharge cycles in a real metal hydride-air battery. The electrochemically and vacuum deposited Co_xO_v/ZrO_2, Co–Ni–Te–O and Co–Te–O films exhibit much higher mass activity compared to $Cu_{0.2}Co_{2.8}O_4$ for both oxygen reduction and evolution reactions. The difference is that the loading of electrochemically and vacuum deposited films is 0.06 mg cm^{-2} only, which is a substantial advantage from a practical viewpoint.

1. Introduction

Oxygen reduction and evolution are basic processes in many environmentally related fields such as H_2/O_2 and direct methanol fuel cells, rechargeable metal-air (M-air) and metal hydride-air (MH-air) batteries, water electrolysis, and chloralkali cells. Unitized regenerative fuel cells are promising dual mode energy storage systems, combining a water splitting electrolyzer for hydrogen and oxygen generation and a fuel cell for their subsequent conversion into electrical energy. A key for such systems is the development of a bifunctional air/oxygen electrode.

However, the oxygen electrode is known to be a strongly irreversible system with a high activation overvoltage in aqueous solutions [1]. Due to this reason, the choice of electrocatalysts for oxygen reactions is limited to four groups of materials: (i) Pt, Ag, Ni with high-area surfaces, (ii) mixed valence oxides of Co, Ni and Mn with a spinel and perovskite crystal structure, (iii) metal sulfides, nitrides and carbides, and (iv) mixed metal oxides catalysts containing Pt, Ir, Ru, Os and Rh. Among these, cobalt and manganese spinels Co_3O_4, $M_xCo_{3-x}O_4$ (M = Cu, Ni) and $Cu_xMn_{3-x}O_4$ are presently being considered as the most promising electrocatalysts in alkaline solutions, because of their relatively high catalytic activity, larger availability and lower cost compared to the noble metals, together with their good corrosion stability [2–5]. Different methods for electrocatalyst preparation have been proposed: low temperature synthesis using inorganic and organic precursors [6–10]; sol–gel processes [11–13]; freeze-drying methods [14]; chemical spray pyrolysis [15]; cathodic sputtering [16]; vacuum evaporation [17–23], and electrochemical deposition [24–29].

Since the reaction proceeds at the three-phase boundary catalyst–electrolyte–gas, it is important to expand the surface area in contact with the electrolyte and the O_2 molecules, dissolved or gaseous.

To solve this problem, two approaches have been applied in this study: (i) preparation of GDEs with different designs, allowing lower catalyst loading, better electronic conductivity and higher corrosion stability, and (ii) preparation and deposition of catalysts as nanopowders or thin films.

Three groups of cobalt oxide based catalysts were synthesized: (i) $Cu_xCo_{3-x}O_4$, as powders (ii) Co–Te–O, Co–Ni–Te–O and (iii)

* Corresponding author. Fax: +359 2 722544.
E-mail address: tvitanov@bas.bg (T. Vitanov).

0378-7753/$ – see front matter © 2008 Elsevier B.V. All rights reserved.
doi:10.1016/j.jpowsour.2008.08.031

Co_xO_v/ZrO_2 as thin films, vacuum and electrochemically deposited, respectively.

Depending on the method of catalyst preparation, GDEs with different design have been produced and studied for oxygen reduction and evolution reactions.

The electrochemical performances of the bifunctional GDEs obtained have been compared.

2. Experimental

2.1. Preparation of the catalysts and gas-diffusion electrodes

The catalysts were synthesized by different methods. $Cu_xCo_{3-x}O_4$ powders were prepared by thermal decomposition at 350 °C of mixed nitrate and carbonate precursors [6].

Thin films of Co–Ni–Te–O and Co–Te–O were deposited by vacuum co-evaporation of Co, Ni and TeO_2 on pressed hydrophobic carbon black representing gas-supplying layer [22]. The films with various thicknesses (100–450 nm) were prepared by co-evaporation of Co, Ni and TeO_2 on stationery substrates under vacuum better than 10^{-4} Pa. TeO_2 is the source of oxygen for CoO and NiO synthesis during the co-deposition. The evaporation of TeO_2 and Ni was carried out from independently heated cells of Knudsen type and that of Co by an electron gun. The condensation rates of each substance within the range 0.01–0.04 $\mu g\,cm^{-2}\,s^{-1}$ were controlled separately during the evaporation using quartz crystal monitors. The amount of the three substances as well as the atomic ratios $R_{Co/Te}$, $R_{Co/Ni}$ and $R_{Co+Ni/Te}$ at each point of the substrate were calculated from data from the crystal monitors.

Co_xO_y and ZrO_2 films were obtained by electrochemical deposition from an absolute ethanol containing 2.3 M LiCl as an electroconducting additive to which 0.3 M $ZrCl_4$ or $CoCl_2$ was added [29,30]. The films were deposited on stainless steel gauze (SS) and on nickel foam (Ni). The cathodic deposition was performed in a voltastatic regime at 22 V for ZrO_2 and 8 V per Co_xO_y layers. Because of relatively low equivalent conductivity of the working electrolyte, it warmed up during the electrolysis. For this reason, the electrochemical deposition was carried out in specially constructed, thermostated electrochemical cell. The cell was kept at a constant temperature of 13 °C (±1 °C) by water-cooling circulation. The deposition time was 30 min, and the thicknesses of the layers were ~2 μm, respectively.

The electrochemical behavior of the powder catalysts were studied on bilayered gas diffusion electrodes, Fig. 1a, with $S = 1\,cm^{-2}$, consisting of gas-supplying layer of hydrophobic carbon black (XC-30) with a loading of $100\,mg\,cm^{-2}$ and an active layer containing $50\,mg\,cm^{-2}$ catalyst and $18\,mg\,cm^{-2}$ of XC-30. The carbon black was hydrophobized with Teflon. The electrodes were prepared by mechanically pressing at $300\,kg\,cm^{-2}$ and 300 °C.

The GDE catalyzed with vacuum deposited catalysts (thin films of Co–Ni–Te–O and Co–Te–O) were prepared by direct deposition of the catalyst on gas-supplying layer, thus creating a ready-to-use gas diffusion electrode, Fig. 1b.

A third design of GDE was used for catalysts prepared electrochemically. They were first deposited on Ni foam and than mechanically pressed at $300\,kg\,cm^{-2}$ and 300 °C on gas-supplying layer of hydrophobic carbon black (XC-30) with a loading of $100\,mg\,cm^{-2}$. To obtain cyclic voltammograms, Co_xO_v/ZrO_2 films were deposited electrochemically on stainless steel gauze CC404.

2.2. Catalyst characterization

The phase composition of the synthesized catalysts, their morphology and surface structure were studied by physical methods for bulk and surface analysis. The chemical compositions of the catalyst deposited on the substrate were determined using an X-ray microanalyzer in a scanning electron microscope (JEOL Superprobe 733 with mounted System 5000-HNU, Japan). X-ray diffractograms were recorded using an Philips APD15 X-ray diffractometer. The average particle size was calculated from XRD peaks using the Scherrer equation [31]. Scanning electron microscopy (Philips 515) was used to examine the surface morphology of the electrodes. The chemical states of the elements in the catalytic films deposited on the gas-supplying layer were studied using X-ray photoelectron spectroscopy (XPS). The measurements were carried out in UHV chamber of the electron spectrometer ESCALAB MkII (VG Scientific, UK). The spectra were exited with an Al Kα source with energy 1486.6 eV. The photoelectron lines of C1s, O1s, Te3d, Co2p and Ni2p were recorded. All spectra were calibrated using C1s line at 285.0 eV as a reference. The specific surface area was measured by low temperature nitrogen adsorption by the BET method.

By steady-state and cyclic voltammetric (CV) cycle life measurement, the electrochemical characterization of the electrodes was performed using equipment consisting of potentiostat–galvanostat provided with a pulse generator (Solartron 1286 electrochemical interface).

The GDEs were tested in a three-electrode cell at room temperature. The electrolyte was 3.5 M KOH, prepared from double distilled water. An Ni plate was used as a counterelectrode. The potential was measured versus an Hg/HgO reference electrode in 3.5 M KOH, with a Luggin capillary closely approaching the tested electrode. Cyclic voltammetry was carried out in the potential region between −1000 and +650 mV vs. Hg/HgO. The experiments were carried out at room temperature under argon purging of the electrolyte. Cathodic polarization curves were measured under a flow of pure oxygen or air.

3. Result and discussion

3.1. Physical characteristics of the catalytic films

Tables 1–3 summarize the physicochemical characteristics of the catalysts studied.

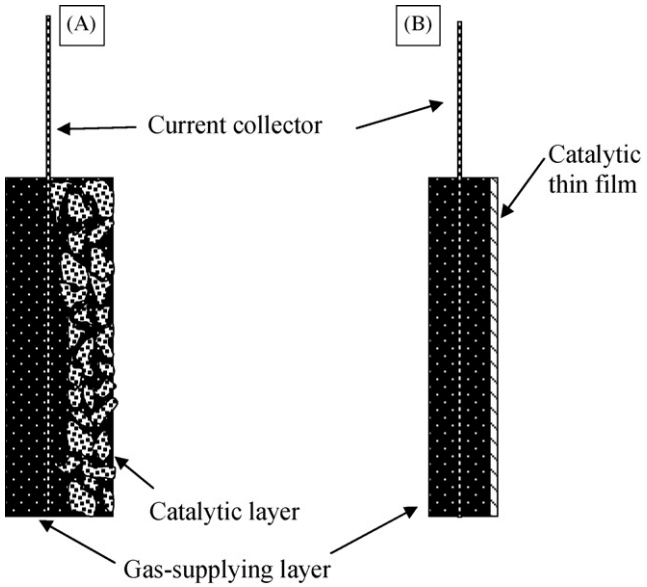

Fig. 1. Schematic view of GDE design: (A) bilayered gas diffusion electrode and (B) GDE catalyzed with vacuum and electrochemically deposited catalysts.

Table 1
Unit cell parameter (a), specific surface area (S), mean particle and Scherrer crystallite sizes of $Cu_xCo_{3-x}O_4$ powders with a spinel structure obtained from nitrate and carbonate precursors

Composition[a]	Preparation temperature (°C)	a (Å)	S_{BET} ($m^2\,g^{-1}$)	Mean particles size (nm)	Scherrer crystallite sizes (nm)
$Cu_{0.2}Co_{2.8}O_4$ (from nitrate)	350	8080	7	≈100	86
$Cu_{0.3}Co_{2.7}O_4$ (from carbonate)	400	8080	75	<50	10

[a] Composition with the best electrochemical characteristics.

Table 2
Structure and composition of vacuum deposited Co–Ni–Te–O and Co–Te–O films

Composition	Preparation temperature (°C)	Structure	Composition
Co–Ni–Te–O $R_{Co/Ni}$ = 4.5	300	Amorphous or nanocrystalline	Co^{2+},Ni^{2+}, Te^{4+},Te^0
Co–Te–O $R_{Co/Te}$ = 1.5	25	Cubic CoO nanocrystals embedded in an amorphous matrix	Co^{2+}, Te^{4+}, Te^0
	300		Co^{2+}, Te^{4+}, Te^0

R, atomic ratio.

The spinel structure of $Cu_xCo_{3-x}O_4$ powders synthesized by the nitrate ($0 \le x \le 0.9$) and carbonate ($x \le 0.5$) methods was confirmed by XRD. The later had higher BET surface area and a smaller particle size than that of the last samples. Data are presented only for the samples with the best electrochemical behavior (Table 1).

The XPS analysis and TEM studies showed that depending on atomic ratio $R_{(Co+Ni)/Te}$ and $R_{Co/Ni}$ the catalyst Co–Ni–Te–O treated at 300 °C is amorphous or nanocrystalline with Co^{2+}, Ni^{2+}, Te^{4+} and Te^0 on the surface. From selected area electron diffraction (SAED) in TEM the as-deposited catalytic films Co–Te–O are generally amorphous with very small nanocrystals of cubic CoO, embedded in the amorphous matrix. The oxidation state of the species is Co^{2+}, Te^{4+} and Te^0. No changes in the chemical state of the films were found after thermal annealing up to 300 °C (Table 2) [23]

XPS analyses of Co_xO_y/ZrO_2 layers were performed. The results are summarized in Table 3. Co^{2+} and Co^{3+} oxidation states were established, with different Co^{2+}/Co^{3+} ratios in layers as deposited at 25 °C and after thermal treatment at 400 °layers were found. The surface concentration of Co^{3+} increases with temperature. Moreover, two types of Co^{2+} species exist in thermally treated layers, most probably from Co^{2+} in $CoZrO_3$ and in Co_3O_4 [29].

3.2. Electrochemical measurements

3.2.1. Cyclic voltammetry

Additional information on the oxidation state on the catalysts surface was obtained by cyclic voltammetry. Fig. 2 shows the CV curve of an immersed $Cu_{0.2}Co_{2.8}O_4$ electrode, synthesized by the nitrate method, in 3.5 M KOH. The curve exhibits a single anodic peak and a corresponding cathodic peak prior to onset of O_2 evolution. However, the cathodic peak is separated from the anodic peak in the cathodic direction; the values of ΔE_p and mean peak potential $E_p = E_{pa} + E_{pc}/2$ being 100 mV and 430 mV (Hg/HgO). Similar voltammetric curves were reported for $NiCo_2O_4$ (ΔE_p = 100 mV and E_p = 420 mV [32], E_p = 400 mV [33] (Hg/HgO)). The observed peaks have been assigned to the formation of a redox couple, $CoO_2/CoOOH$ on the surface under potential cycling conditioned, via the following reaction [33].

$$CoOOH + OH^- \leftrightarrow CoO_2 + H_2O + e^-$$

Fig. 3 shows the CV curve of an immersed $Cu_{0.3}Co_{2.7}O_4$ prepared by the carbonate method in 3.5 M KOH. The two peaks on the curve correspond to reactions as those for the $Cu_{0.2}Co_{2.8}O_4$ electrode synthesized by the nitrate method. The chemical stability of $Cu_{0.3}Co_{2.7}O_4$ obtained from carbonates is also demonstrated in Fig. 3. It is seen that after three months exposure to air the catalyst surface is deactivated (curve b), most probably due to carbonatization. It can be reactivated by an anodic polarization at a potential of oxygen evolution or by a thermal treatment at 400 °C (curve c).

The redox states of the cobalt ions on the surface of vacuum and electrochemically deposited cobalt oxide catalysts are depicted with the peaks in the CV curves in Figs. 4 and 5. Cyclic voltammograms of Co–Te–O a GDE, fresh and thermally treated at different temperatures are given in Fig. 4a [23]. The electrodes have optimal catalyst loading of 0.2 mg cm^{-2} and atomic ratio $R_{Co/Te}$ = 1.5. In comparison, (Fig. 4b), the curves of gas-diffusion membrane (GDM), Te and TeO_2 make no contribution to the peaks observed for Co–Te–O films. CV curves exhibit several very broad, not well-defined peaks, prior to oxygen evolution. The first single anodic peak a1, observed only for a fresh GDE thermally treated at 100 °C

Table 3
Composition of electrochemically deposited Co_xO_y films

Preparation temperature (°C)	Composition
25	Co^{2+}, Co^{3+}
	Co^{2+}/Co^{3+} = 2.4
400	Co^{2+} (two types), Co^{3+}
	Co^{2+}/Co^{3+} = 0.34

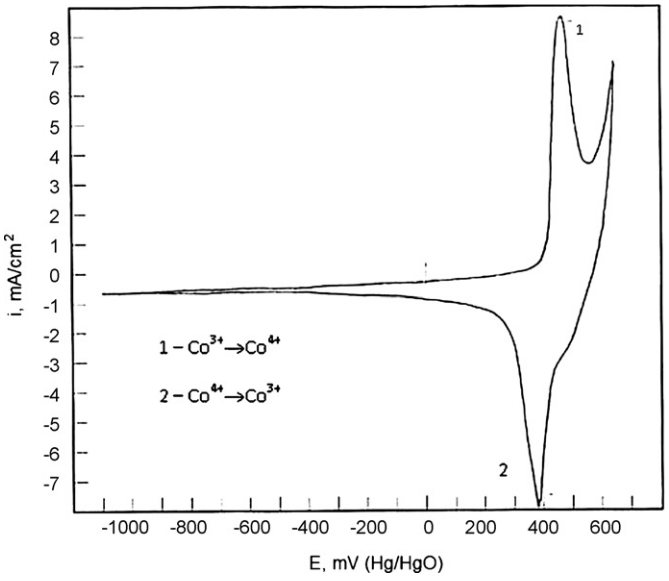

Fig. 2. Cyclic voltammogram of immersed $Cu_{0.2}Co_{2.8}O_4$ (from nitrate) electrode; 100 mV s^{-1}; 3.5 M KOH.

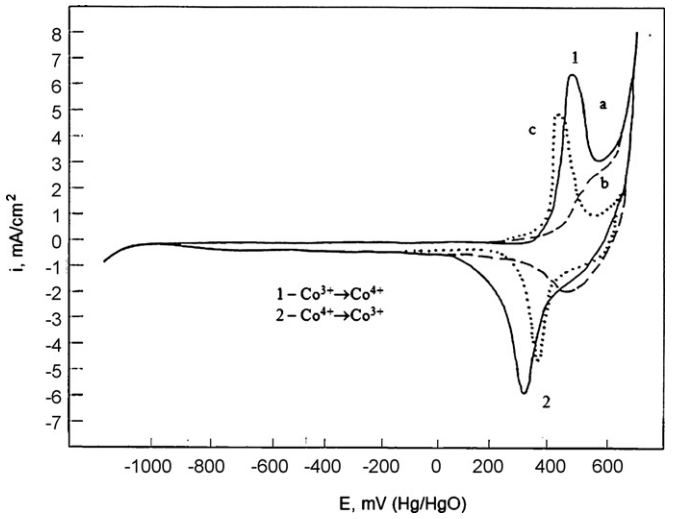

Fig. 3. Cyclic voltammogram of immersed $Cu_{0.3}Co_{2.7}O_4$ (from carbonate) electrode; 100 mV s^{-1}; 3.5 M KOH. (a) Initial, (b) after 3 months, and (c) after 3 months and anodic polarization.

with a maximum at −50 mV is assigned most probably to a redox transition of CoO/CoOOH with calculated potential of −54 mV vs. Hg/HgO [34]. The pair of peaks a2/c2 may be associated with the formation of CoO/CoO_2 redox couple with a calculated potential at +195 mV and/or $Co\{OH)_2/CoO_2$ at +254 mV [34]. The third anodic

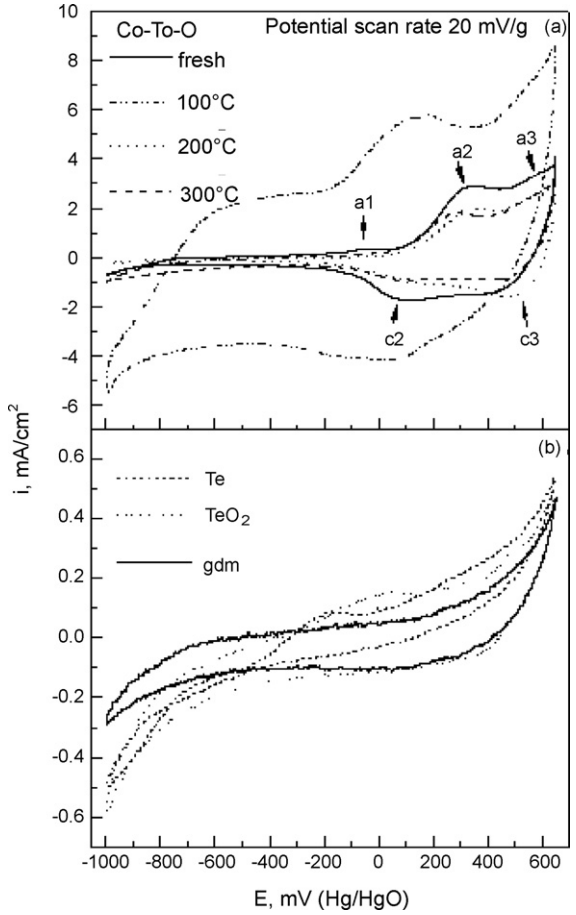

Fig. 4. Cyclic voltammmogram of immersed Co–Te–O electrode, as deposited; 100 mV s^{-1}; $R_{Co/Te}$ = 1.5; 3.5 M KOH.

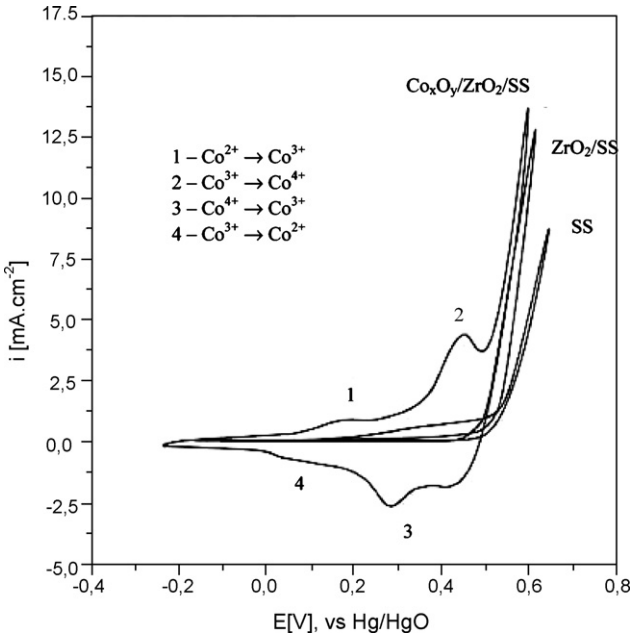

Fig. 5. Cyclic voltammogram of immersed Co_xO_y/ZrO_2electrode on stainless steel gauze (Co_xO_y/ZrO_2/SS); 200 mV s^{-1}; 3.5 M KOH. For sake of comparison, voltammograms of pure stainless steel (SS) and ZrO_2 deposited on stainless steel (ZrO_2/SS) are also given.

peak a3 is not well expressed, but it becomes clearer on increasing the scan rate. It is noted that all peaks discussed are more clearly defined in CV curves on planar substrate (Pt). The potential at which the peak a3 and its corresponding cathodic peak c3 appear are an indication that the redox transition $CoOOH/CoO_2$ at +562 mV vs. Hg/HgO occurs [34].

A cyclic voltammogram of electrochemically deposited Co_xO_y/ZrO_2/SS immersed electrode with a catalyst loading of 0.06 mg cm^{-2} is presented in Fig. 5. For comparison, the curves for ZrO_2 and stainless steel gauze (SS) are given in Fig. 5. It is seen that they do not make any contribution to the peaks observed for Co_xO_y/ZrO_2 films. The CV curve exhibits several broad peaks prior to oxygen evolution. The two anodic peaks E_{p1} = +0.15 V and E_{p2} = +0.42 V (Hg/HgO) on the curve, according to [34,35] correspond to the reactions 1 ($Co^{2+} \rightarrow Co^{3+}$) and 4 ($Co^{3+} \rightarrow Co^{2+}$) and the peaks 2, 3 to the reactions 2 ($Co^{3+} \rightarrow Co^{4+}$) and 3 ($Co^{4+} \rightarrow Co^{3+}$), respectively. The "pseudo" peak at a potential more positive as

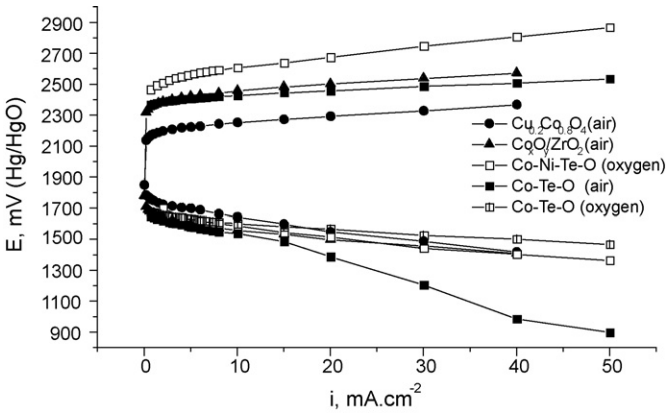

Fig. 6. Steady-state current–voltage curves of $Cu_{0.2}Co_{2.8}O_4$ powder, Co–Ni–Te–O, Co–Te–O and Co_xO_y/ZrO_2 gas-diffusion electrodes in air or O_2, 3.5 M KOH.

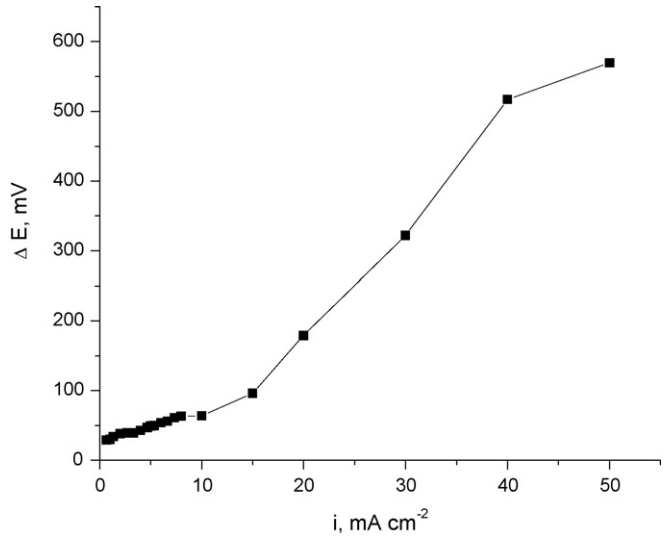

Fig. 7. ΔE–i curve of Co–Te–O GDE in air and O_2.

compared to the peak 3 potential most probably indicates a splitting of the cathodic process [36].

A main feature of the CV curves for the vacuum and electrochemically thin film electrodes are the broad peaks, most probably as a result of the heterogeneity of the size distribution of the active surface sites [37] or to the high degree of porosity or/and roughness, which affects the energy of the active sites, thus leading to the broadening of the peak [38]. Besides, new peaks appear on the curves—a1 and a2/c2 (Fig. 4) and 1, 4 (Fig. 5). The latter peaks are missing on chemically synthesized samples. These features are evidence of different surface composition of the two types of electrocatalysts.

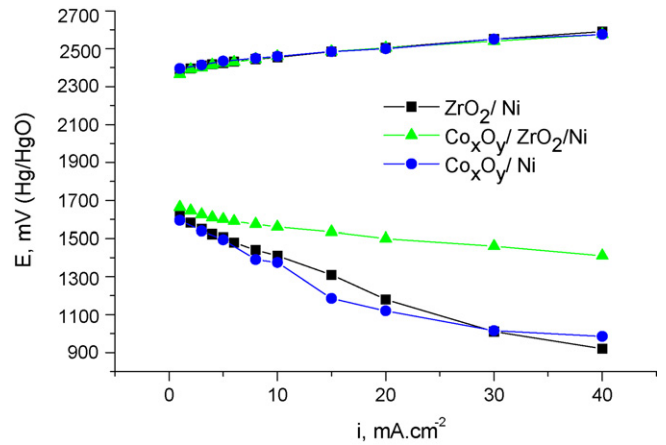

Fig. 8. Current–voltage curves, i–E, of Co_xO_y/ZrO_2/Ni-, Co_xO_y/Ni- and ZrO_2/Ni-air gas-diffusion electrodes.

Table 5
Electrode potentials of $Cu_xCo_{3-x}O_4$, Co–Ni–Te–O, Co–Te–O and Co_xO_y/ZrO_2 gas-diffusion electrodes in air or in O_2 (i = 40 mA cm^{-2})

Composition	Loading (mg cm^{-2})	E_c (mV)[a]	E_a (mV)[a]
$Cu_{0.2}Co_{2.8}O_4$ (air) (nitrate)	50	1690	2200
$Cu_{0.3}Co_{2.7}O_4$ (air) (carbonate)	50	1550	2350
Co–Ni–Te–O (O_2) $R_{Co/Ni}$ = 4.5	0.07	1420	2870
CoO–TeO_2 (air) $R_{Co/Te}$ = 1.5	0.06	1020	2520
Co_xO_y/ZrO_2 (air)	<0.06	1435	2600

[a] E vs. Hg/HgO.

3.2.2. Steady-state measurements

The electrochemical activity of the different catalysts is depicted by the steady-state current–voltage curves shown in Fig. 6. This compares current–voltage curves for $Cu_{0.2}Co_{2.8}O_4$ powder, electrochemically deposited Co_xO_y/ZrO_2 and vacuum deposited Co–Ni–Te–O, Co–Te–O thin films, where oxygen reduction for Co–Te–O is tested in air and oxygen, while for Co–Ni–Te–O is tested in oxygen alone. It is clear that the GDE using vacuum deposited Co–Te–O shows lower performance when operating on air. This can be explained by gas transport hindrances in the GDE, as is shown in Fig. 7. This presents the ΔE–i curves for GDE in air and oxygen which are considered to be criteria for gas transport limitations. The high value of ΔE in air and oxygen shows that GDEs with vacuum deposited Co–Te–O are not optimized as fuel cell electrodes.

The electrochemical parameters of the curves of all tested catalysts (some of them not shown in Fig. 6) at low current density (Tafel region) are presented in Table 4. The activity (estimated as electrode potential at a constant current) for the OR reaction increases in the order:

$$\text{Co–Te–O} \leq Co_xO_y/ZrO_2 < Cu_{0.3}Co_{2.7}O_4(\text{fromcarbonate}) < Cu_{0.2}Co_{2.8}O_4(\text{fromnitrate}),$$

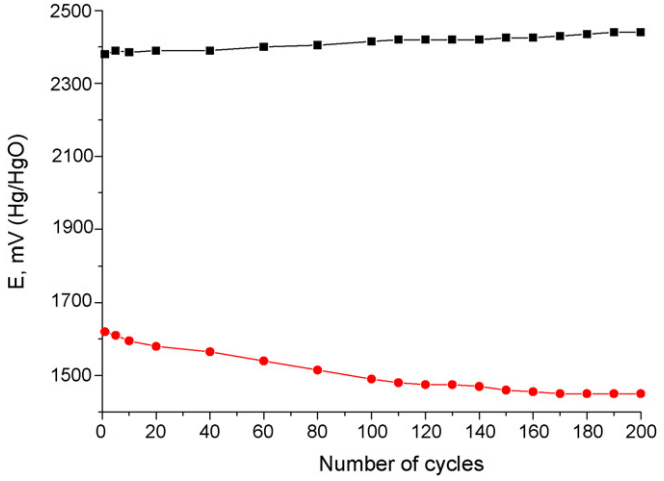

Fig. 9. Charge–discharge cycles of $Cu_{0.3}Co_{2.7}O_4$-air gas-diffusion electrode; $i_{ch} = i_{dis}$ = 20 mA cm^2, 25 °C, 3.5 M KOH. ■ Anodic, ● cathodic.

Table 4
Electrochemical characteristics of $Cu_xCo_{3-x}O_4$, Co–Ni–Te–O, Co–Te–O, Co_xO_y/ZrO_2 gas diffusion electrodes at low current density in air or in O_2 (Tafel region)

Composition	Loading (mg cm^{-2})	i = 6 mA cm^{-2} E_c (mV)[a]	E_a (mV)[a]	b_c (mV)	b_a (mV)
$Cu_{0.2}Co_{2.8}O_4$ (air) (nitrate)	50	1770	2160	60	150
$Cu_{0.3}Co_{2.7}O_4$ (air) (carbonate)	50	1740	2330	100	150
Co–Ni–Te–O (O_2) $R_{Co/Ni=4.5}$	0.07	1620	2470	66	128
Co–Te–O (air) $R_{Co/Te=1.5}$	0.06	1585	2425	63	47
Co_xO_y/ZrO_2 (air)	<0.06	1600	2440	220	85

[a] E vs. Hg/HgO.

Table 6
Apparent and mass electrode activity (i_{app} and i_m) as current density at E = 1520 and 2520 mV for oxygen reduction and evolution reactions

Electrode	Loading (mg cm^{-2})	i at E (mV [Hg/HgO])			
		E = 1520 mV		E = 2520 mV	
		i_{app} (mA cm^{-2})	i_m (mA mg^{-1})	I_{app} (mA cm^{-2})	I_m (mA mg^{-1})
$Cu_{0.2}Co_{2.8}O_4$ (nitrate), air	50	27	0.54	50	1
$NiCo_2O_4$ (sol–gel) [34]	2.8	–	–	324	115
NiO–CoO (low temp.) [35], air	14	25	1.8	38	2.7
Co–Ni–Te–O (vacuum), O_2	0.07	20	286	23	328
Co–Te–O (vacuum), O_2	0.05	40	800	36	720
Air		6.3	126		
Co_xO_y/ZrO_2 (electrochem), air	0.06	20	333	20	333

and for the oxygen evolution (OE) reaction:

$$\text{Co–Ni–Te–O} < Co_xO_y/ZrO_2 \approx \text{Co–Te–O} < Cu_{0.3}Co_{2.7}O_4(\text{fromcarbonate}) < Cu_{0.2}Co_{2.8}O_4(\text{fromnitrate}).$$

The observed orders of catalyst activity could result from a number of factors: (i) catalyst loading, (ii) chemical composition, (iii) structural effects (electronic, crystallographic, surface structure on atomic level, distribution of the cations in different crystal lattices), (iv) electronic conductivity, (v) geometrical properties (particle size, roughness/morphology factor of the catalytic layer), (vi) hyper–hypo-d-electronic interaction between the catalyst components (synergistic effect).

At low current density we can explain the better performance of powder catalysts for both reactions as due to the high catalyst loading (50 mg cm^{-2}) compared to the vacuum and electrochemically deposited samples (0.07 and 0.06 mg cm^{-2}, respectively).

The activity of the vacuum evaporated films may be ascribed to a nanoparticle effect (Table 3). On the other hand, the catalytic effect measured on electrochemically deposited layers could be explained as a hyper–hypo-d-electronic interaction between Co_3O_4 with a hyper-d- and ZrO_2 with a hypo-d-electronic structures. This is supported by the current–voltage curves in Fig. 8 showing that in the Tafel region the value of the current density (c.d.) on Co_xO_y/ZrO_2/Ni electrode is higher than that of both the ZrO_2/Ni and Co_xO_y/Ni electrodes.

At higher current density (i = 40 mA cm^{-2}, Table 5) the order of electrode activity for the OE reaction is the same as that at low current density, while for the OR reaction the order is

$$\text{Co–Te–O} \ll Co_xO_y/ZrO_2 < Cu_{0.3}Co_{2.7}O_4 < Cu_{0.2}Co_{2.8}O_4$$

This order of electrochemical performances most probably is determined by transport limitations for the OR reaction. It seems that the diffusion conditions in active layers made from powder catalysts as well as from electrochemically deposited thin films results in the same order of performance even though the catalyst loading on these electrodes differs by three orders of magnitude. Under the same conditions the electrode performance of vacuum deposited Co–Te–O is most probably reduced due to a non-optimized three-phase boundary (Fig. 7).

A gas-diffusion electrode-catalyzed with $Cu_{0.3}Co_{2.7}O_4$ was tested in a real metal hydride-air battery. The charge and discharge current densities were $i_{ch} = i_{dis}$ = 20 mA cm^{-2} for the bifunctional GDE. The time of charge (oxygen evolution) and time of discharge (oxygen reduction) was 16 was 8 h. 200 charge–discharge cycles, and stable current–voltage characteristics were achieved (Fig. 9).

It is interesting to compare the electrocatalytic activity of the cobalt oxides studied with that of cobalt electrocatalysts prepared by other methods. As far the apparent current density depends on the catalyst loading, more informative would be the comparison of both the apparent (i_{app}, mA cm^{-2}) and the mass activity (i_m, mA mg^{-1}). Because of the lack of literature data for catalyst loading, the comparison in Table 6 is made only with two cobalt electrocatalysts, prepared by sol–gel [39] and low temperature techniques [40]. The analysis of the data in Table 6 shows that vacuum evaporated and electrochemically deposited cobalt oxide electrocatalysts prepared by us exhibit much higher mass activity for both reactions, probably due to a maximum use of catalytic material. This is a substantial advantage from a practical viewpoint.

4. Conclusion

1. Gas-diffusion electrodes with 50 mg cm^{-2} loadings of $Cu_{0.2}Co_{2.8}O_4$ and $Cu_{0.3}Co_{2.7}O_4$ powders exhibit a good apparent catalytic activity in oxygen reduction and evolution reactions. GDEs with $Cu_{0.3}Co_{2.7}O_4$ powder exhibit stable current–voltage characteristics after 200 charge–discharge cycles in air gas-diffusion electrodes. The lower mass activity of these electrodes most probably is due to the larger particles size as well as to the smaller surface area in contact with the electrolyte and O_2 molecules.
2. The vacuum and electrochemically deposited Co–Ni–Te–O, Co–Te–O and Co_xO_y/ZrO_2 catalytic films exhibit high mass activity and electrochemical stability for both oxygen reduction and evolution reactions despite a minimal catalyst loading of about 0.05–0.07 mg cm^{-2}
3. Application of catalytic thin films allows the preparation of bifunctional GDEs with new designs. The thin active layers determine maximum use of catalytic material. These types of electrodes have less catalyst loading, which is a substantial advantage from a practical point of view.

References

[1] E.J.M. O'Sullivan, E.J. Calvo, in: R.G. Compton (Ed.), Electrode Kinetic Reaction, Elsevier, Amsterdam, 1987, p. 274.
[2] P. Rasiyah, A.C.C. Tseung, J. Electrochem. Soc. 130 (1983) 2384.
[3] H. Nguyen Cong, P. Chartier, J. Brenet, J. Appl. Electrochem. 7 (1977) 383.
[4] H. Nguyen Cong, P. Chartier, J. Brenet, J. Appl. Electrochem. 7 (1977) 395.
[5] A. Daghetti, G. Lodi, S. Trasatti, Mater. Chem. Phys. 8 (1983) 1.
[6] I. Nikolov, R. Darkaoui, E. Zhecheva, R. Stoyanova, N. Dimitrov, T. Vitanov, J. Electroanal. Chem. 429 (1997) 157.
[7] J. Haenen, W. Visscher, E. Barendrecht, J. Electroanal. Chem. 208 (1986) 273.
[8] J. Marco, J. Gancedo, M. Gracia, J.L. Gautier, E. Rios, F. Berry, J. Sol. State 153 (2000) 74.
[9] H. Garapuca, M. Pereira, F. Cocta, Mater. Res. Bul. 25 (1990) 1183.
[10] W. King, A. Tseung, Electrochim. Acta 19 (1974) 485.
[11] E. Svegl, B. Orel, M.G. Hutchins, K. Kalcher, J. Electrochem. Soc. 143 (1996) 1532.
[12] M.L. Baydi, M.G. Poillerat, J.L. Gautier, G.L. Rehspringer, J.F. Koenig, P. Chartier, J. Solid State Chem. 109 (1994) 278.
[13] M.L. Baydi, S.K. Tiwari, R.N. Singh, J.L. Rehspringer, P. Chartier, J.F. Koenig, M.G. Poillerat, J. Solid State Chem. 116 (1995) 157.
[14] P. Rasiyah, A. Tseung, J. Electrochem. Soc. 130 (1983) 2384.
[15] R.N. Singh, J.F. Koenig, G. Poillerat, P. Chartier, J. Electroanal. Chem. 314 (1991) 241.
[16] B. Nkeng, G. Poillerat, J.F. Koenig, P. Chartier, B. Lefez, J. Lopitaux, M. Lenglet, J. Electrochem. Soc. 142 (1995) 1777.

[17] P. Nkeng, J.F. Koenig, J. Gautier, P. Chartier, G. Poilerat, J. Electroanal. Chem. 402 (1996) 81.
[18] F.K. Shokoohi, J.M. Tarascon, B.J. Wilkens, D. Guyomard, C.C. Chang, J. Electrochem. Soc. 139 (7) (1992) 1845.
[19] K.H. Hwang, S.H. Lee, S.K. Joo, J. Electrochem. Soc. 141 (12) (1994) 3296.
[20] H. Benqlilou-Moudden, G. Blondiaux, P. Vinatier, A. Levasseur, Thin Solid Films, 333 (1998) 16.
[21] B. Wang, J. Bates, F. Hart, B. Sales, R. Zuhr, J. Robertson, J. Electrochem. Soc. 143 (10) (1996) 3203.
[22] V. Rashkova, S. Kitova, I. Konstantinov, T. Vitanov, Electrochim. Acta 47 (2002) 1555.
[23] V. Rashkova, S. Kitova, T. Vitanov, Electrochim. Acta 52 (2007) 3794.
[24] J. Ismail, M.F. Ahmed, P. Vishnu Kamath, J. Power Sources 36 (1991) 507.
[25] E. Hayes, B. Bellingam, H. Mark Jr., A. Galal, Electrochim. Acta 41 (2) (1996) 337.
[26] C. Barbero, G. Planes, M. Miras, Electrochem. Commun. 3 (2001) 113.
[27] D. Carrigan, R. Bendert, J. Electrochem. Soc. 136 (3) (1989) 723.
[28] A. Mansour, C. Melendres, J. Wong, J. Electrochem. Soc. 145 (4) (1998) 1121.
[29] I. Valov, D. Stoychev, T. Vitanov, Unpublished results.
[30] I. Valov, D. Stoychev, Ts. Marinova, Electrochim. Acta 47 (2002) 4419.
[31] H.P. Klug, L. Alexander (Eds.), X-ray Procedures for Polycrystalline and Amorphous Materials, Wiley/Intrsciense, New York, 1980.
[32] R. Singh, J. Koenig, G. Poillerat, P. Chartier, J. Electrochem. Soc. 137 (1990) 1408.
[33] M. Hamdani, J.F. Koenig, P. Chartier, J. Appl. Electrochem. 18 (1988) 568.
[34] W. Behl, J. Toni, J. Electroanal. Chem. 31 (1971) 63.
[35] M. Pourbaix, Atlas d'equilibres electrochemique, Gauthiers-Villars, Paris, 1963.
[36] R. Boggio, A. Carugatti, S. Trasatti, J. Appl. Electrochem. 17 (1987) 828.
[37] S. Trasatti, J. in, P.N. Lipkowski, Ross (Eds.), The Electrochemistry of Novel Materials, VCH, Weinheim, 1994.
[38] M. Santana, L.D. Faria, J. Boodts, Electrochim. Acta 49 (2004) 1925.
[39] R.N. Singh, J.P. Pandey, N.K. Singh, B. Lal, P. Chartier, J.F. Koenig, Symposium, Electrochemistry and Materials: Synthesis and Characterization Symposium, 50th ISE Meeting, Pavia, Italia, 5–10 September, 1999.
[40] S. Gamburzev, W. Zhang, O.A. Velev, S. Srinivasan, A.J. Appleby, J. Appl. Electrochem. 28 (1998) 545.